Plasmoid formation in global GRMHD simulations and AGN flares

Antonios Nathanail[1], ⋆ Christian M. Fromm[1,2], Oliver Porth [3], Hector Olivares[1], Ziri Younsi[4], Yosuke Mizuno[1] and Luciano Rezzolla[1,5]

[1]*Institut für Theoretische Physik, Goethe Universität Frankfurt, Max-von-Laue-Str.1, 60438 Frankfurt am Main, Germany*
[2]*Max-Planck-Institut für Radioastronomie, Auf dem Hügel 69, D-53121 Bonn, Germany*
[3]*Astronomical Institute Anton Pannekoek, Universeit van Amsterdam, Science Park 904, 1098 XH, Amsterdam, The Netherlands*
[4]*Mullard Space Science Laboratory, University College London, Holmbury St. Mary, Dorking, Surrey, RH5 6NT, UK*
[5]*School of Mathematics, Trinity College, Dublin 2, Ireland*

6 February 2020

ArXiv:2002.01777, 5 Feb 2020

Accepted in MNRAS, will be published in

Volume 495, Issue 2, June 2020, Pages 1549–1565

Miljenko Čemeljić, SHAO Visiting Scientist (PIFI)

Outline

- Introduction
- Simulations setup
- Numerical simulations
- Results, discussion
- Conclusions

Introduction-observational motivation

-Relativistic jets are observed in high-energy sources, from gamma-ray bursts (GRB) to active galactic nuclei (AGNs). They can be launched from magnetic processes around black holes.

-Observations of rapid variability of X-ray/gamma-ray flares in blazars with timescales from several minutes to a few hours pose severe constraints on the particle acceleration timescale and the size of the emission region (e.g., Aharonian et al. 2007; Albert et al. 2007).

-Fast variable flares may origin from a small region with a size of the order of a few Schwarzschild radii, launching fast moving “needles” within a slower jet or from jet within a jet (Levinson 2007; Begelman et al. 2008). Such flares require very rapid particle acceleration.

Introduction

-Current sheets generated throughout the jet by the turbulence induced by instabilities are naturally the sites for magnetic reconnection. They are structured by large sheets of alternating magnetic-field polarity and can be very efficient in particle acceleration.

-The initial configuration fragments at the current sheet layer and produces chains of magnetic “plasmoids” (or “magnetic islands”, Loureiro et al. 2007, Uzdensky et al. 2010): quasi-spherical regions that contain relativistic particles and have a large magnetization (ratio between the magnetic and rest-mass energies).

-Instability driving the accretion in magnetized disks is thought to be the magneto-rotational instability (MRI, Balbus & Hawley 1991), through which plasma and fields are advected, to form magnetized winds and jets.

Introduction

-Simulations show that structure of the outflows is determined by the geometry of magnetic field. It is also essential for energy dissipation through MHD instabilities and reconnection. Turbulent nature of the accretion process produces and advects onto the black hole loops of magnetic field of different polarity - interaction of such loops provides the sites for formation of current sheets. Turbulence results in the large scale magnetized jets of variable electromagnetic power.

-Magnetically dominated jets accelerate efficiently the bulk of the plasma while keeping much of the energy stored into the field itself. In such cases, magnetic reconnection is efficient in dissipating some of the magnetic energy-it has been proposed to explain GRB and AGN emission (di Matteo1998; Zhang & Shu 2011; Giannios & Sironi 2013; Dionysopoulou et al. 2015).

Introduction

-Studies with different magnetic field configurations revealed that if the launched jets are weak and turbulent, or powerful and collimated, mostly depends on the initial magnetic-field geometry (Beckwith et al. 2008, 2009)

-The magnetic loops can be lifted in the surface of the disk because of buoyancy, like the Rayleigh-Taylor instability. It can change the topology of the magnetic field throughout the jet. Being turbulent, they will not respect any symmetry across the equatorial plane-causing the differences in the wind properties above and below the equatorial plane.

-It was shown in numerical studies that for the production of a steady outflow (especially its power), the nested-loop poloidal magnetic-field structure produces the relativistic jets (Gammie et al. 2004; De Villiers et al. 2005; McKinney 2006). Depending on the initial magnetic field strength, the efficiency of the energy extraction from BH can go beyond 100% efficiency, resulting in very powerful outflows in the case of magnetically arrested disks (MAD, Igumenshchev et al. 2003; Narayan et al. 2003; Tchekhovskoy et al. 2011). Various combinations of loops were investigated with regions of alternating magnetic-field polarity (Parfrey et al. 2015, Contopoulos et al. 2015, 2018).

Numerical simulations

-Because of importance of plasmoid formation and evolution in the dynamics and energetics of relativistic jets, authors made a study of properties of formed plasmoids in general-relativistic conditions of accretion flows around black hole. They search for cases leading to the formation of current sheets and to magnetic reconnection.

-The accretion torus (in 2D general-relativistic ideal-MHD simulations) with a varying number of poloidal magnetic loops of alternating polarity is initialized, and the results compared with those obtained with the nested-loop setup typically used in the literature:

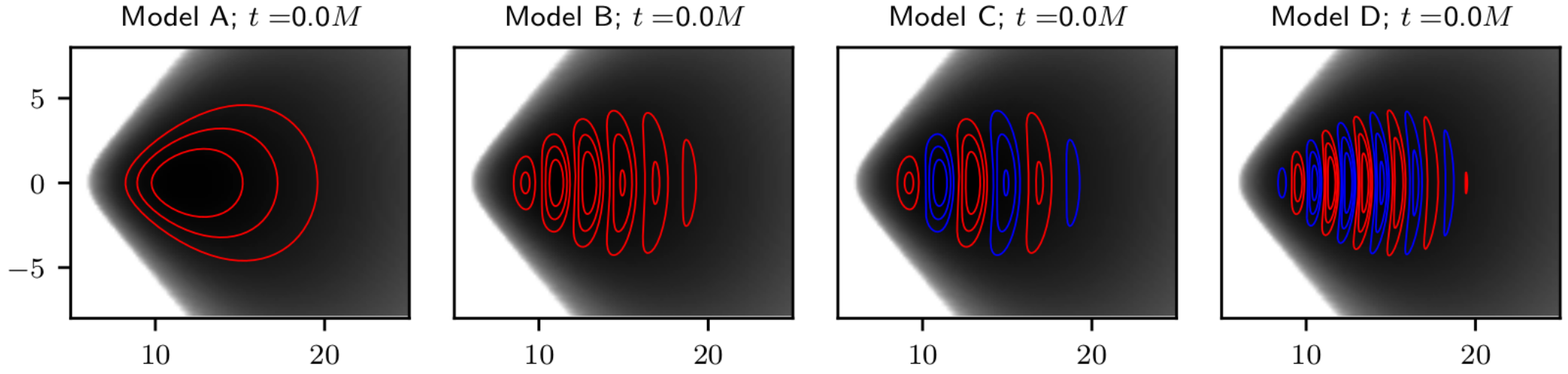

Figure 1. Initial magnetic-field configuration for the four models. from left to right is `Model A`, `Model B`, `Model C` and `Model D`. The different colors of the magnetic loops indicate their direction, where red is clockwise and blue counterclockwise. In the background the density of the torus is shown in black.

Simulations-setup

fully tested and compared with codes with similar capabilities Porth et al. (2019). BHAC solves the general-relativistic MHD equations

$$\nabla_\mu(\rho u^\mu) = 0\,, \qquad A_\phi \propto \mathcal{A}\times\mathcal{B}$$
$$\nabla_\mu T^{\mu\nu} = 0\,, \qquad \mathcal{A} = \max(\rho/\rho_{\max} - 0.2, 0)$$
$$\nabla_\mu {}^*F^{\mu\nu} = 0\,, \qquad \mathcal{B} = \cos((N-1)\theta)\sin(2\pi\,(r - r_{\rm in})/\lambda_r)$$

where ρ is the rest-mass density, u^μ the fluid 4-velocity, $T^{\mu\nu}$ the energy momentum tensor and ${}^*F^{\mu\nu}$ is the dual of the Faraday tensor. Our simulations are performed in two spatial dimensions. The code makes uses of fully adaptive mesh-refinement (AMR) techniques and of the constrained-transport method (Del Zanna et al. 2007) to preserve a divergence-free magnetic field (Olivares et al. 2019).

BHAC in ideal MHD, with second-order high-resolution shock-capturing finite-volume methods. No physical resistivity, dissipation of the magnetic energy is generated entirely by the finite numerical resolution. The results qualitatively similar in all resolutions, so authors claim they will be robust, and valid even in the resistive simulation, producing outgoing, gravitationally unbound plasmoids.

-Simulations start from a torus in hydrodynamic equilibrium (Fishbone & Moncrief 1976) with constant specific ang.momentum ℓ=4.28 around a Kerr BH, spin a= J/M^2 = 0.93, (J, M are ang. mom. & mass). Torus r_{in} = 6 r_g, and r_{out}=12 r_g , with grav. radius r_g=M (with G = c = 1). Torus is threaded by poloidal magnetic field loops, defined by the vector potential A_Φ.

-ρ_{max} is the maximum rest-mass density in the torus. Parameter N≥1 sets the number of loops, and λ_r sets the loops' characteristic length scale (and the polarity). Parameters are varied to produce various initial magnetic-field topologies. In most of the runs a logarithmic grid in the radial direction is used, with the domain extending to 2500 r_g.

Simulations-results

-Model A includes the typical nested loop magnetic-field topology. Model B consists of a multi-loop structure where all loops have the same polarity. Models C,D have a multi-loop structure where each loop has an alternate polarity. The loops of Model B and Model C have a similar width, whereas in Model D the loops have a smaller size.

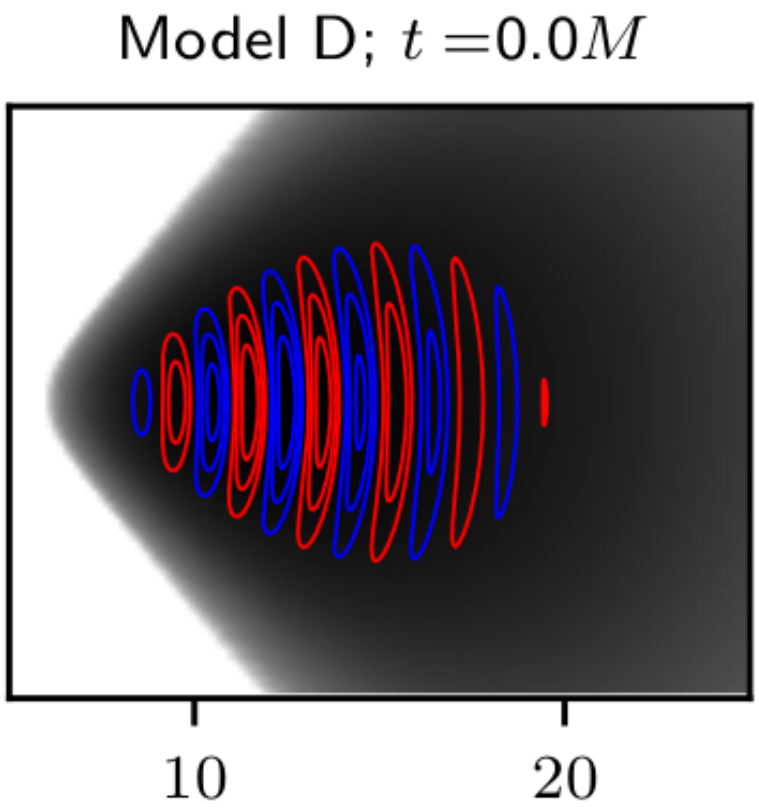

-In models C and D, several resolutions were used to check the impact on the activation and saturation of the MRI (-in the Appendix B).

-For the two models with alternate polarity loops, C and D, a set of 3D simulations was run, evolving up to t = 5 × 10^3 M, sufficiently long to capture all the important features of each simulation, and short enough for not being concerned about the decaying poloidal magnetic field, which takes place in axisymmetry as a consequence of the decay of turbulence (The anti-dynamo theorem, Cowling 1933: axisymmetric, ideal MHD systems do not have any dynamo to replenish the decaying B; Sądowski et al. 2015).

model	N	λ_r	A_ϕ	$N_r \times N_\theta \times N_\phi$ (base res.)	$N_r \times N_\theta \times N_\phi$ (2 × base res.)	$N_r \times N_\theta \times N_\phi$ (4 × base res.)	$N_r \times N_\theta \times N_\phi$ (6 × base res.)
Model A	1	–	$A_\phi = \mathcal{A}$	$1024 \times 512 \times 1$	$2048 \times 1024 \times 1$	$4096 \times 2048 \times 1$	
Model B	3	4	$A_\phi = \mathcal{A} \times \lvert\mathcal{B}\rvert$	$1024 \times 512 \times 1$	–	–	–
Model C	3	4	$A_\phi = \mathcal{A} \times \mathcal{B}$	$1024 \times 512 \times 1$	$2048 \times 1024 \times 1$	$4096 \times 2048 \times 1$	–
Model D	3	2	$A_\phi = \mathcal{A} \times \mathcal{B}$	$1024 \times 512 \times 1$	$2048 \times 1024 \times 1$	$4096 \times 2048 \times 1$	$6144 \times 3072 \times 1$

Comparison of the results

-Authors determine features in the plasma dynamics that emerge from different initial magnetic-field topologies. The mass-accretion rate and the accreted magnetic flux onto the BH are shown (in blue line is model A):

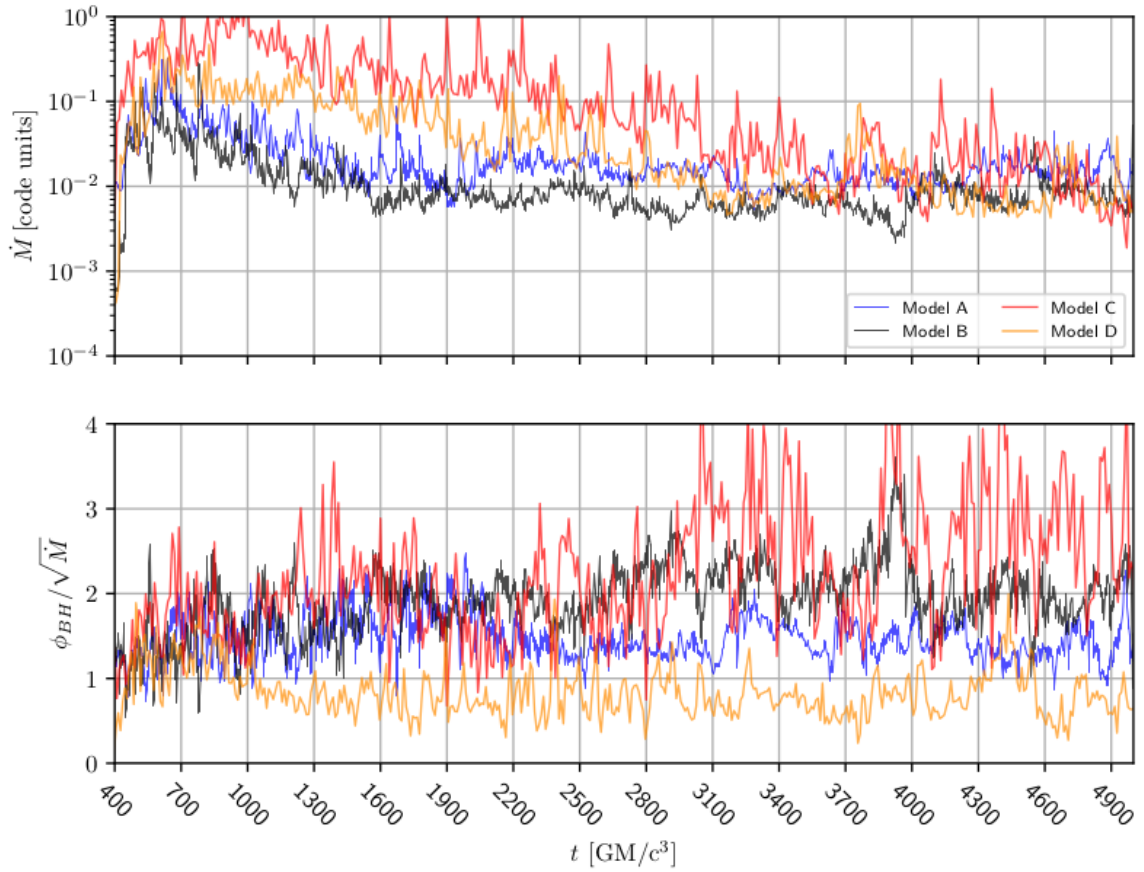

$$\dot{M} := \int_0^{2\pi} \int_0^{\pi} \rho u^r \sqrt{-g}\, d\theta d\phi$$

$$\phi_{\rm BH} := \frac{1}{2} \int_0^{2\pi} \int_0^{\pi} |B^r| \sqrt{-g} d\theta d\phi$$

After t~ 3000 M , the accretion rate in all models relaxes to a roughly constant value. In Model C and D the mass-accretion rate remains roughly constant till 12000 M, in the high-resolution runs, so a stationary turbulent state in the torus is reached.

.

-For Model A, the magnetic flux is roughly constant. It it far below the usual MAD saturation limit $\varphi_{BH}=\varphi_{max}\approx 15$ (Tchekhovskoy et al. 2011), a net magnetic flux needed for energy extraction from the black hole (Blandford & Znajek 1977).

Figure 2. Upper panel: the rate of mass accreted through the black-hole horizon, Lower panel: the magnetic flux accumulated on the black-hole horizon. For models `Models A, B, C` and `D`, reporting the high-resolution run for each model (i.e., at the base resolution for `Models A` and `B`, at 4× the base resolution for `Model C`, and at 6× for `Model D`).

Comparison of the results

-Magnetic flux of one polarity is brought towards the horizon of the black hole but also the magnetic flux of the opposite polarity reaches the vicinity of the horizon, thus annihilating the previous one and reducing the overall flux across the horizon. Fluctuations in this overall behaviour are stronger in the two cases where the initial loops have larger width, i.e., Models B and C . In these cases, the evolution of the magnetic flux shows both a short dynamical timescale – as magnetic flux is brought to the horizon – but also a longer timescale reflecting the amount of time needed for the whole loop to be partly annihilated and as a result reduce the magnetic flux on the horizon.

-The magnetic flux in Models B and C is at all times higher than in the other two cases.

-Even if the magnetic flux in Model C is three or four times larger than Model A , a magnetic funnel is never produced due to the continuous magnetic flux annihilation.

Comparison of the results

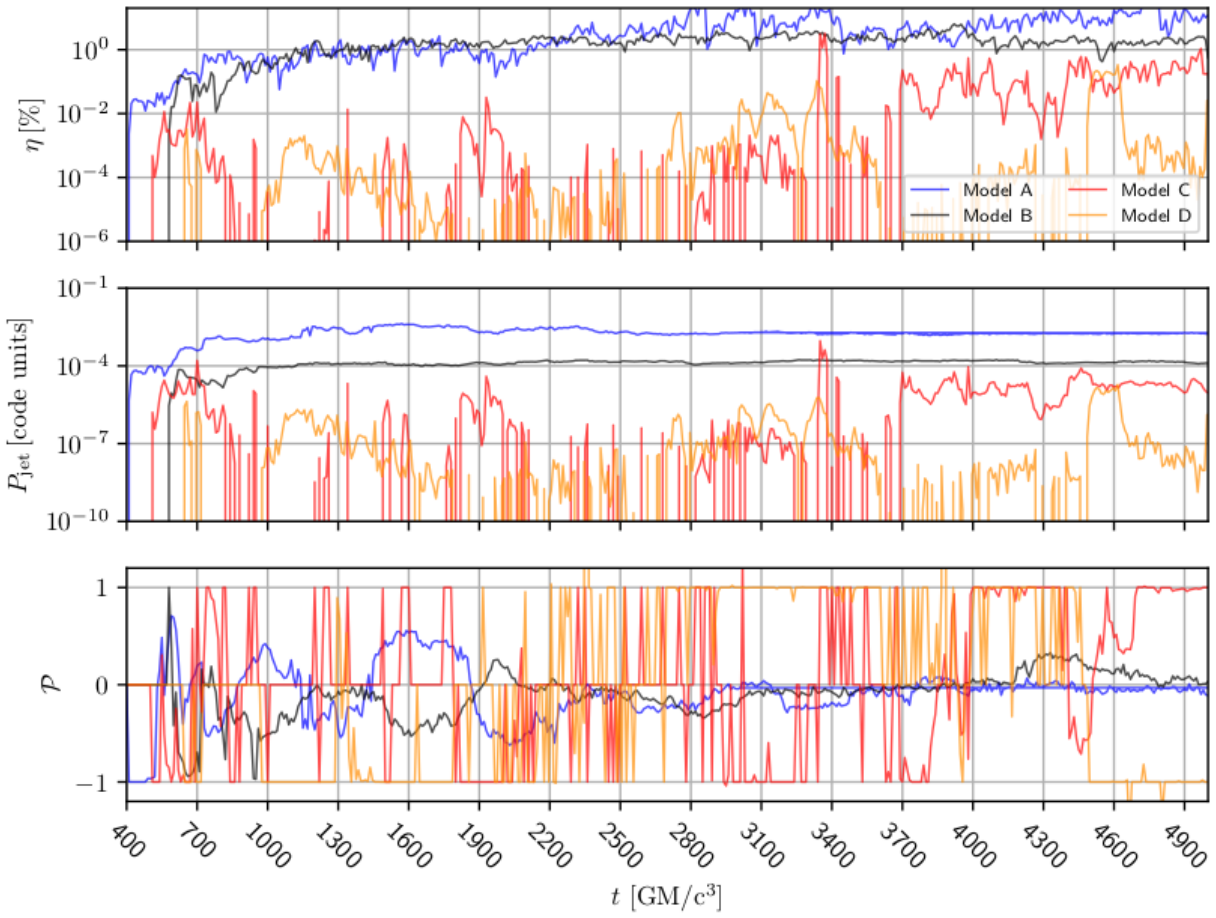

Figure 3. Upper panel: the efficiency of the outflow as defined in Eq. (8), Middle panel: the power of the jet as defined in Eq. (7), Lower panel: the difference in the power, of the upper and the lower jet as defined in Eq. (9).For models `Model A, B, C` and `D`, referring to the highest-resolution run for each model.

$$P_{\rm jet} := \int_0^{2\pi}\int_0^{\pi}(-T^r_t - \rho u^r)\sqrt{-g}d\theta d\phi$$

$$\eta := P_{\rm jet}/\dot{M}$$

$$\mathcal{P} := \frac{P_{\rm jet,u} - P_{\rm jet,l}}{(P_{\rm jet,u} + P_{\rm jet,l})}$$

Outflows depose energy at infinity. This can be measured through the energy flux that passes through a 2-sphere placed at $50r_g$. where the integrand in P_{jet} is set to zero if everywhere on the integrating surface $\sigma \leq 1$. The efficiency of the jet is η. The contribution in the power from the upper and the lower jet is measured by the jet asymmetry P with indices for u(pper) and l(ower) jets.

Comparison of the results

-In the plots, the jet is visualised by use of the the magnetization parameter $\sigma = B^2/\rho$ as the low-density, strong magnetic-field region with $\sigma > 1$. Here is shown zoom close to the BH, with the green line showing the contour of $\sigma = 1$.

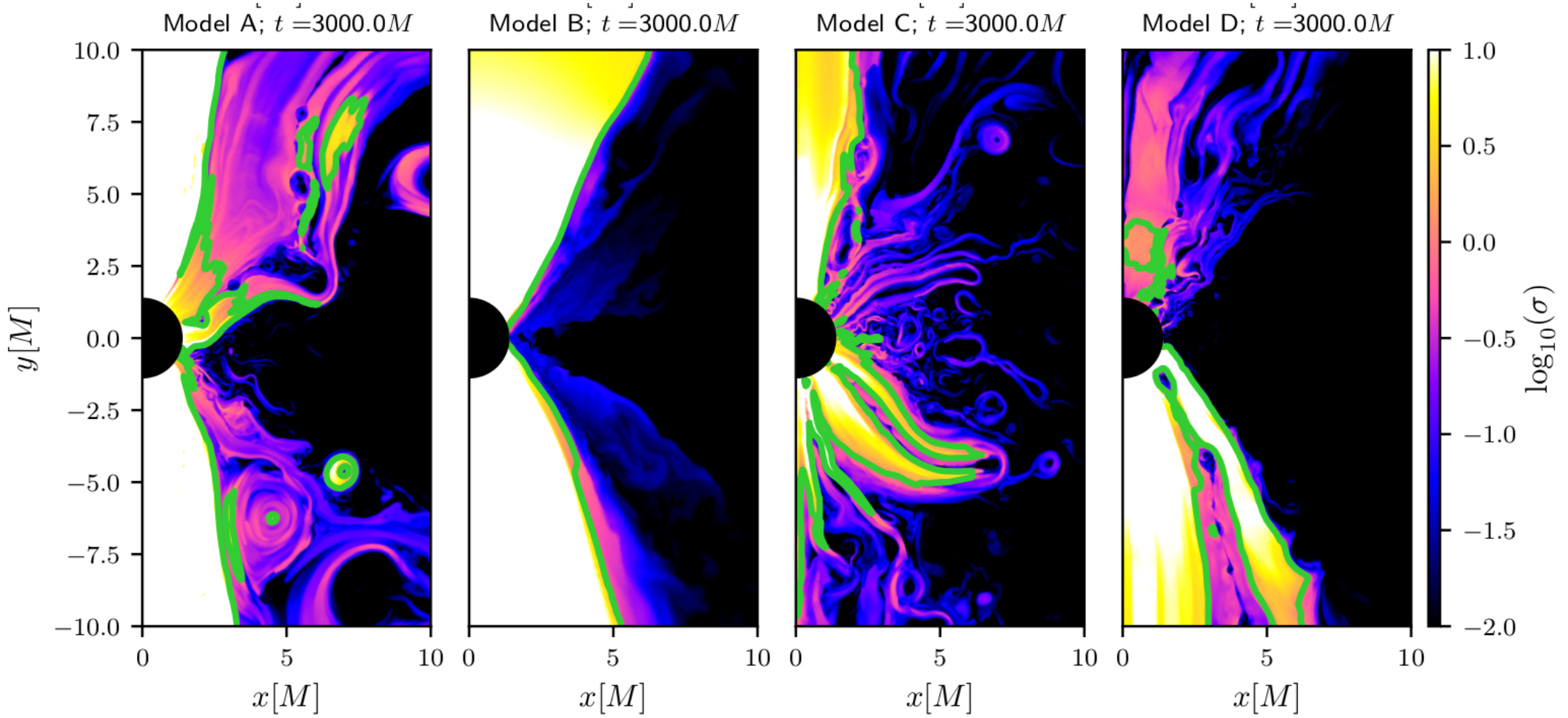

Comparison of the results

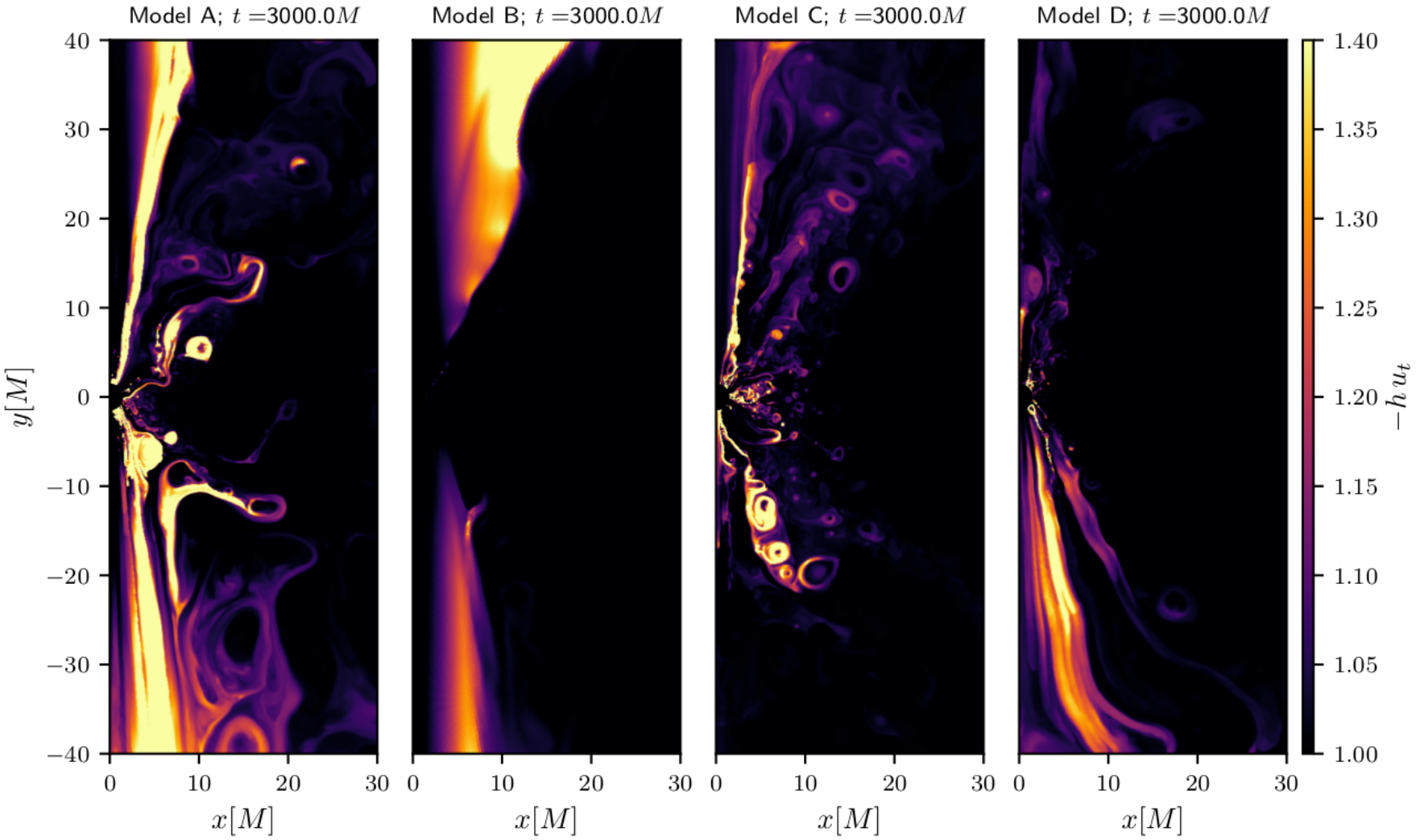

Figure 5. Bernoulli constant $-hu_t$ at time $t = 3000\,M$, any feature/fluid element which is not black in the figure is unbound/outgoing. The two models on the left have a well-defined and uniform regions where matter is unbound, whereas the models on the right have smaller unbound regions mostly localised in plasmoids. The resolutions are: base resolution for `Model B`, 4× base resolution for `Models A`, `C` and `D`.

In models A and B the magnetization is large and the fluid in funnel regions is expected to be accelerated and to become gravitationally unbound. The Bernoulli criterion measures it: a fluid element is defined to be unbound if it has $hu_t \leq -1$, where h is the specific enthalpy of the fluid.

Comparison of the results

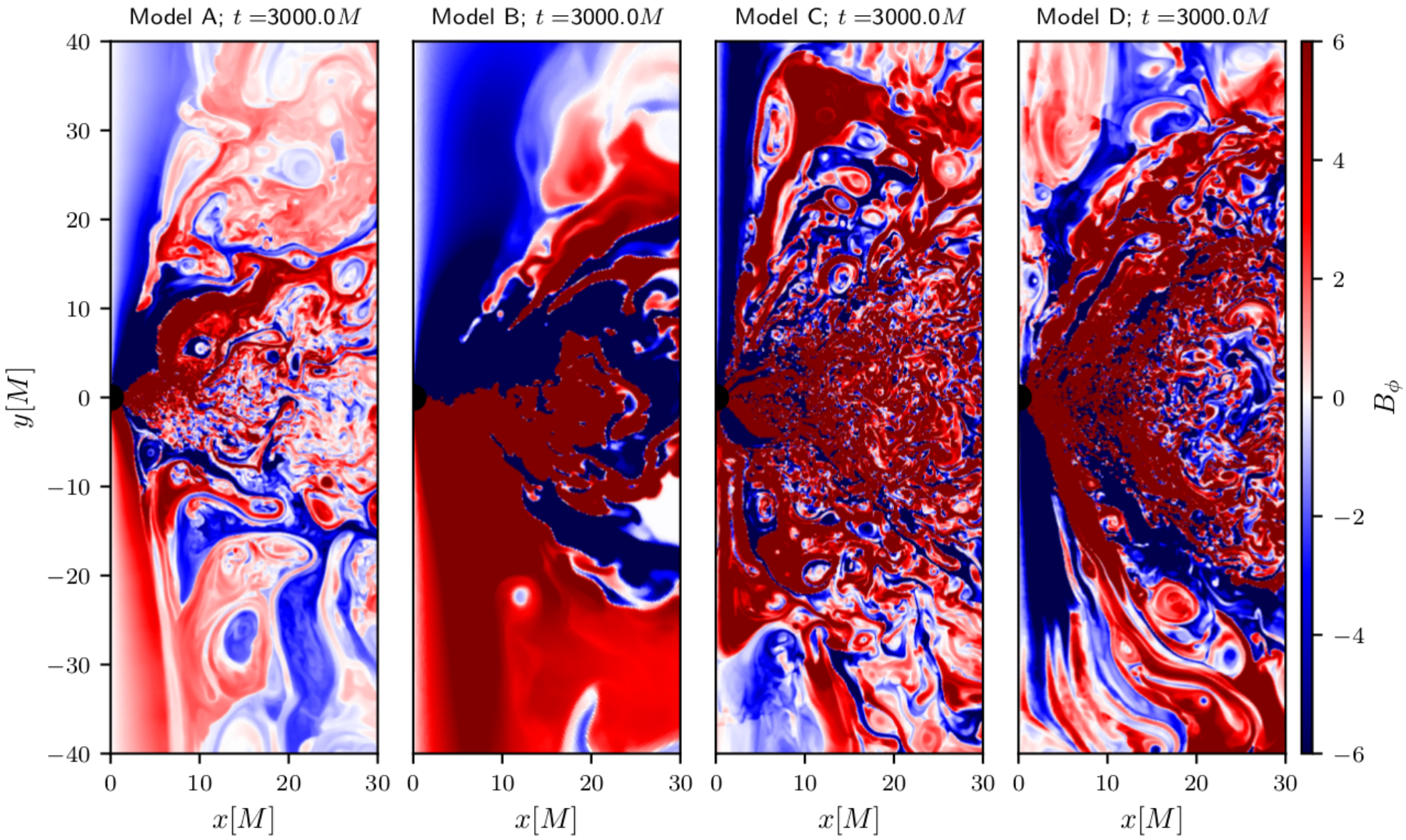

Figure 6. The B_ϕ component of the magnetic field for the four models at time $t = 3000\,M$. The red and blue regions denote regions where the magnetic field has different polarity. The resolutions are: base resolution for `Model B`, 4× base resolution for `Models A`, `C` and `D`.

Comparison of the results

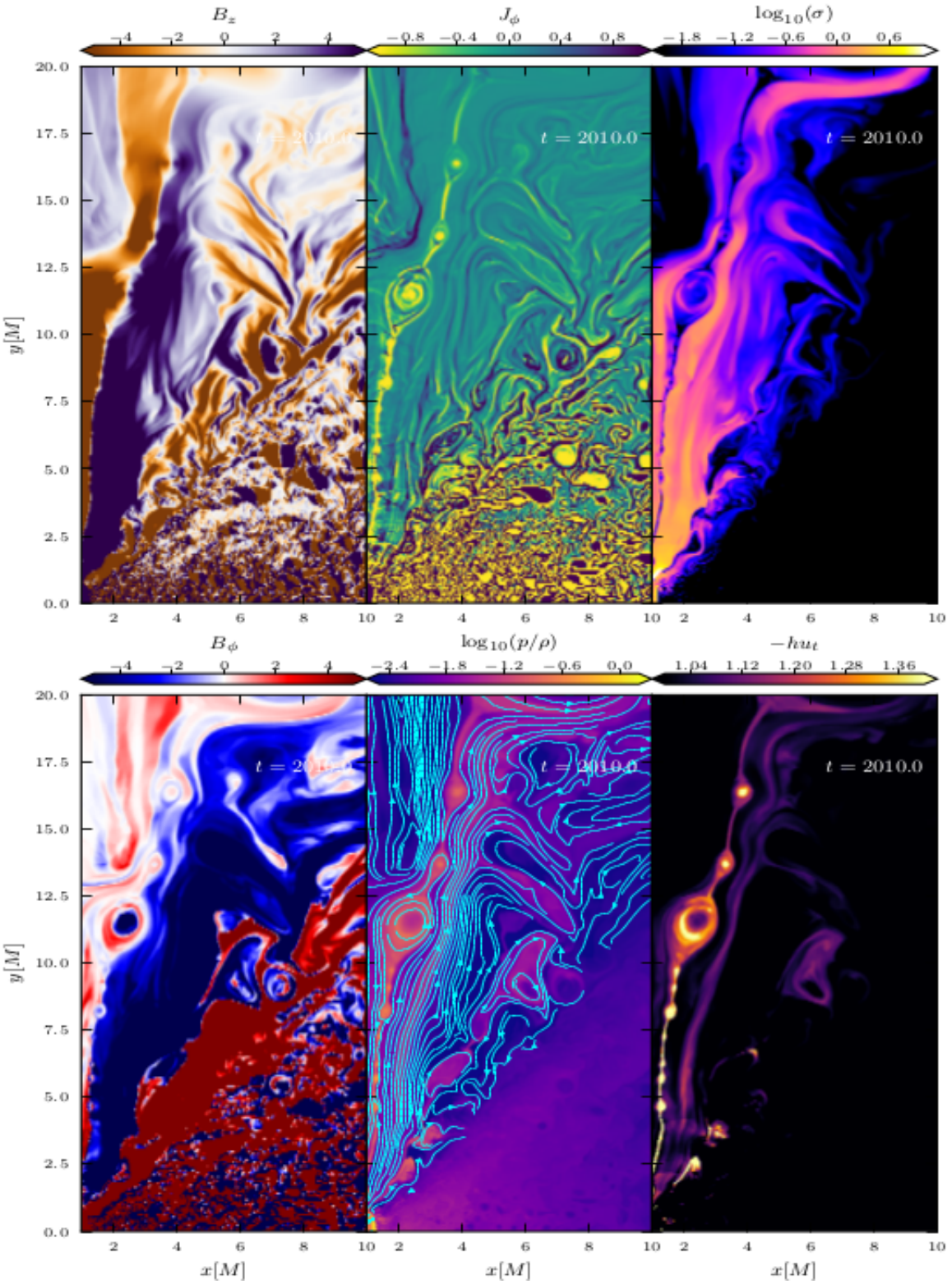

Properties of the current-sheet structure formed in Model D at time t = 2010 M . First row, from left to right: Bz , Jφ and log_10 (σ), whereas in the second row: Bφ , p/ρ, and −hut . In the middle panel of the second row, poloidal magnetic-field lines are illustrated in cyan (for clarity, magnetic-field lines are not shown in the dense torus region).

Comparison of the results

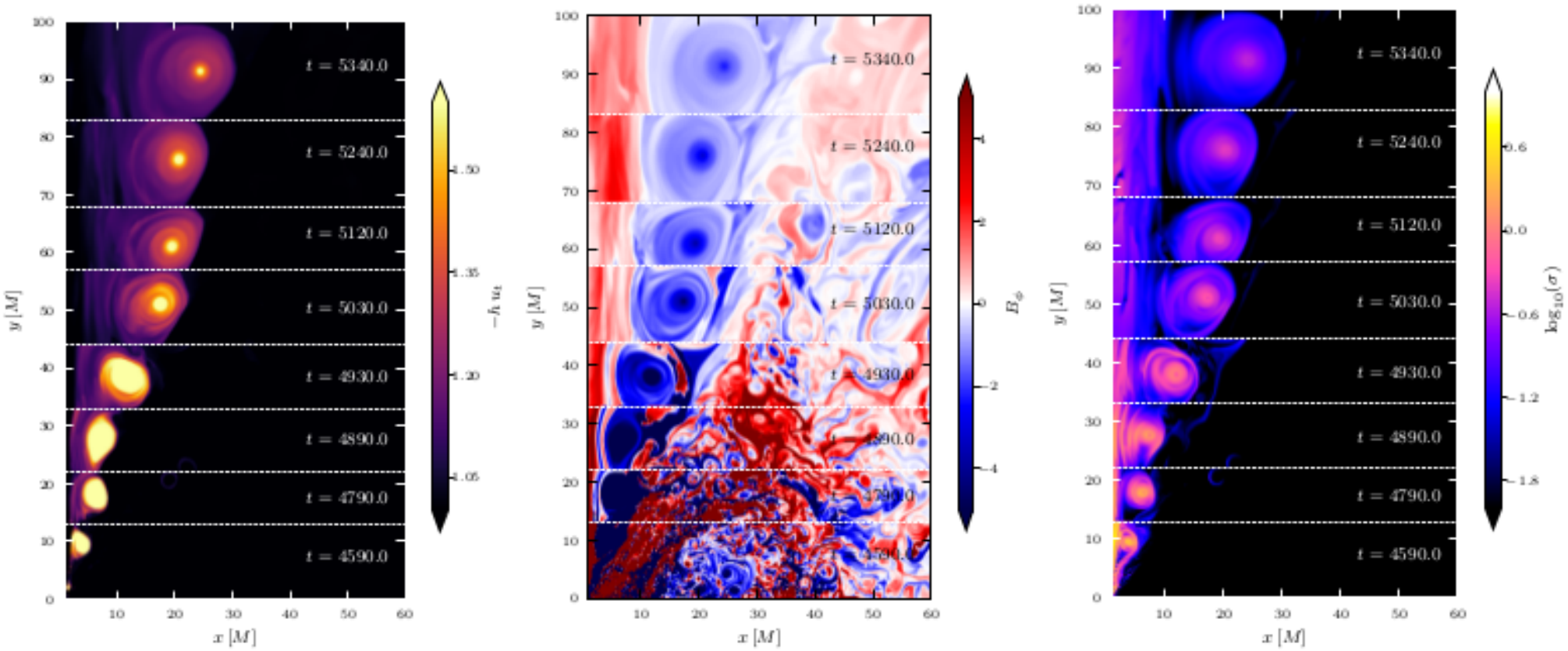

Figure 9. Spacetime diagram showing the evolution of a detected plasmoid from `Model D`, through the Bernoulli constant $-hu_t$, the B_ϕ and the magnetization parameter σ at times from $t = 4590 - 5340\,M$.

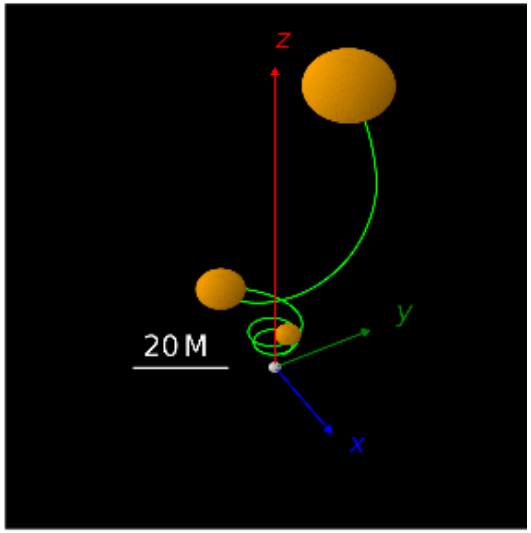

3D reconstruction of the trajectory of the outward moving plasmoid shown in Fig. 9 after integrating in time the velocity of its core, including the azimuthal component.

Measuring the plasmoids

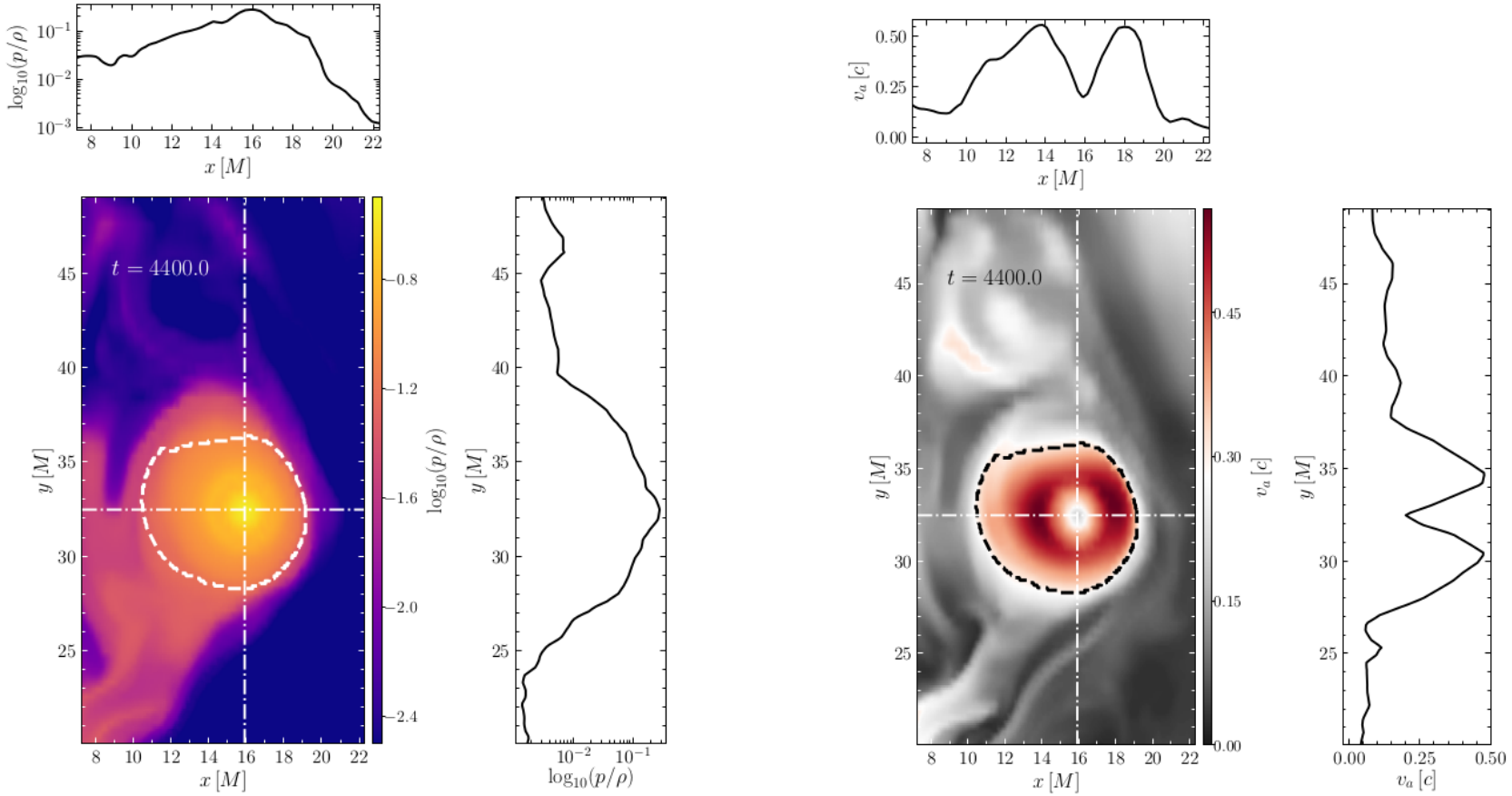

Figure 12. Detection of a plasmoid from `Model D` for either the temperature proxy (left panels) or the Alfvèn speed (right panels). The two (horizontal and vertical) dashed lines pass though the center of the plasmoid. The two subplots show exactly the cuts made by these lines through the plasmoid.

Measuring the plasmoids

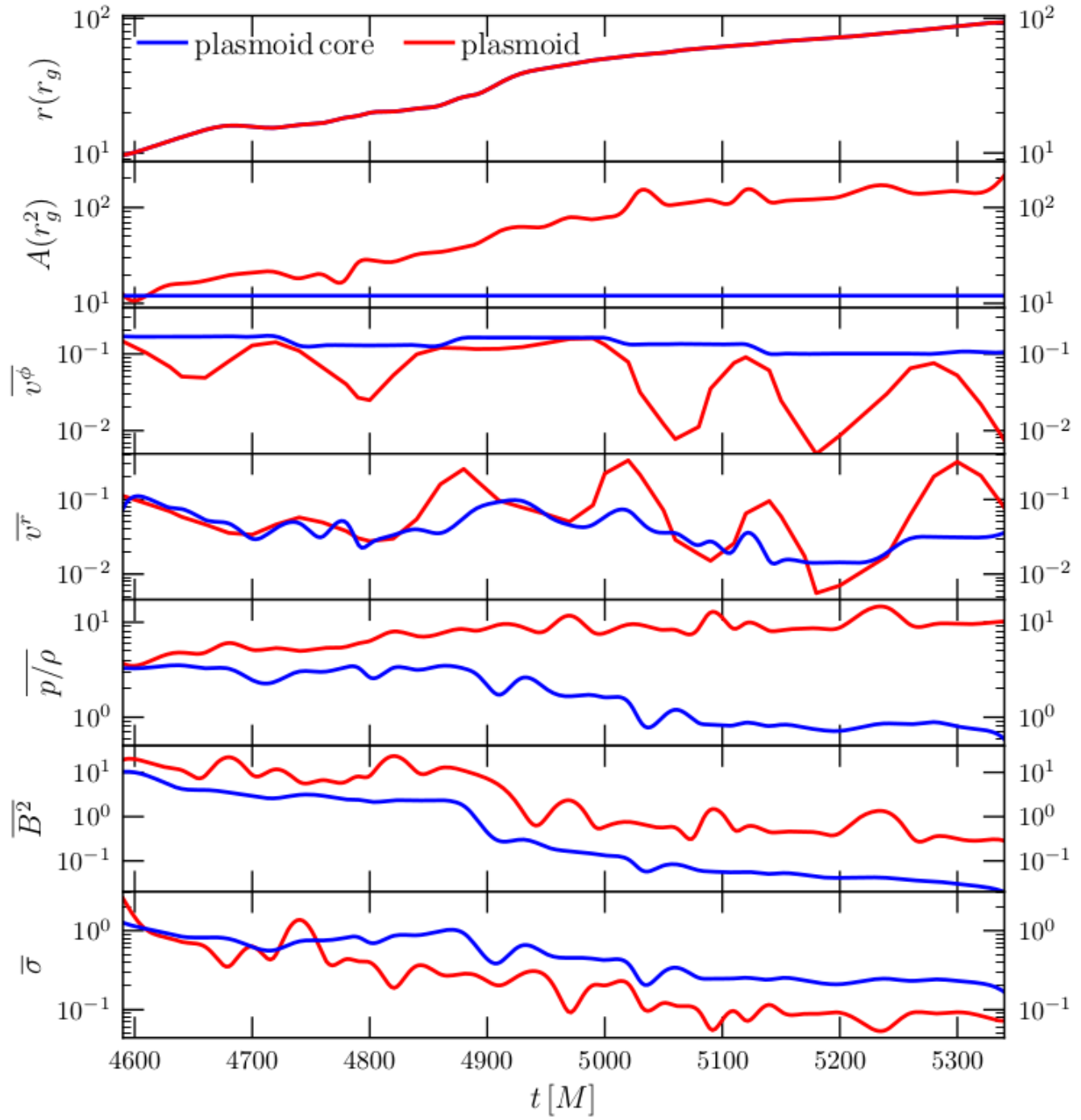

Evolution of a detected plasmoid from Model D, from t=4590 − 5340 M. The evolution of the whole plasmoid is shown in red and the evolution of the core of the plasmoid in blue. The first panel shows the distance of the plasmoid from the black hole, whereas the second panel the evolution of the area that encloses the plasmoid, which for the core of the plasmoid is constant. The next five panels show the average σ, p/ρ, B^2 , Vφ and Vr respectively, for the plasmoid and its core. The last panel shows the distance of the core of the plasmoid from the black hole.

Conclusions

-When employing an initial magnetic-field configuration that does not consist of the standard single poloida field loop, a stationary jet configuration does not form.

-Tori with initial magnetic loops with alternating polarity (multi-loop initial topology; Models C and D) evolve dramatically different from the dynamics of small scale loops of the same polarity (Model B). Same-polarity loops quickly reconnect to form a large loop with resulting flow similar to the single loop setup (Model A).

-Opposite-polarity loops preserve their small coherence length, giving rise to copious plasmoids in the ensuing turbulent evolution. Magnetic fields with small coherence lengths are advected to the black hole and give rise to fluctuating jets of low average power (10^−4 − 10^−3 times the jet power with tori having the same polarity) but large variability. Rarely, the fluctuating jet power can reach or exceed the typical jet power in the same polarity cases which amounts to 1 − 10% of the accretion power in Model A scenario. In addition, tori having a multi-loop initial topology produce an accretion flow that does not produce a stationary magnetized jet, but a series of regions of poloidal and toroidal magnetic fields with alternating polarities. At the boundaries of these regions, reconnection can take place and generate plasmoids with large magnetization.

-Most of the plasmoids are accreted to the black hole or remain in the high-density torus. Plasmoids generated in reconnection layers with relatively high magnetization, i.e., $\sigma >= 0.3$, are outward moving in the funnel region and gravitationally unbound.

Conclusions-flaring

-Recent observations of flaring activity and variability from AGNs hint that very rapid particle acceleration is required and that the emission region is relatively compact, few Schwarzschild radii (Levinson 2007; Begelman et al. 2008; Ghisellini & Tavecchio 2008; Giannios et al. 2009). Magnetic reconnection in the vicinity of a black hole can provide both rapid particle acceleraion and a compact emission region.

-Presented simulations show that the models with an initial (opposite polarity) multi-loop magnetic geometry are varying in the power lost via outflows. It is because of the accretion, forcing small scale loops transport near the black hole, especially to the polar regions, where the magnetization is larger – and reconnect, releasing the magnetic energy. The produced plasmoid chains are filled with relativistic particles, which can represent an additional source of variability.

-Large plasmoid chains impact the emitted power of the outflow, increasing it to more than two orders of magnitude at times (Ponti et al. 2017; Do et al. 2019).
These plasmoids have nonzero angular momentum, and exhibit orbital motion. This might relate them to the recent observations of orbiting material near the galactic center (Abuter et al. 2018).

Thank you